

Tunable Perfect Absorption Structures Based on Cavity Coupling and Plasmon Hybrid Mode

Volume 13, Number 2, April 2021

Yuanhang Zhao

Zizheng Li

Qiang Li

Kun Wang

Jinbo Gao

Ke Wang

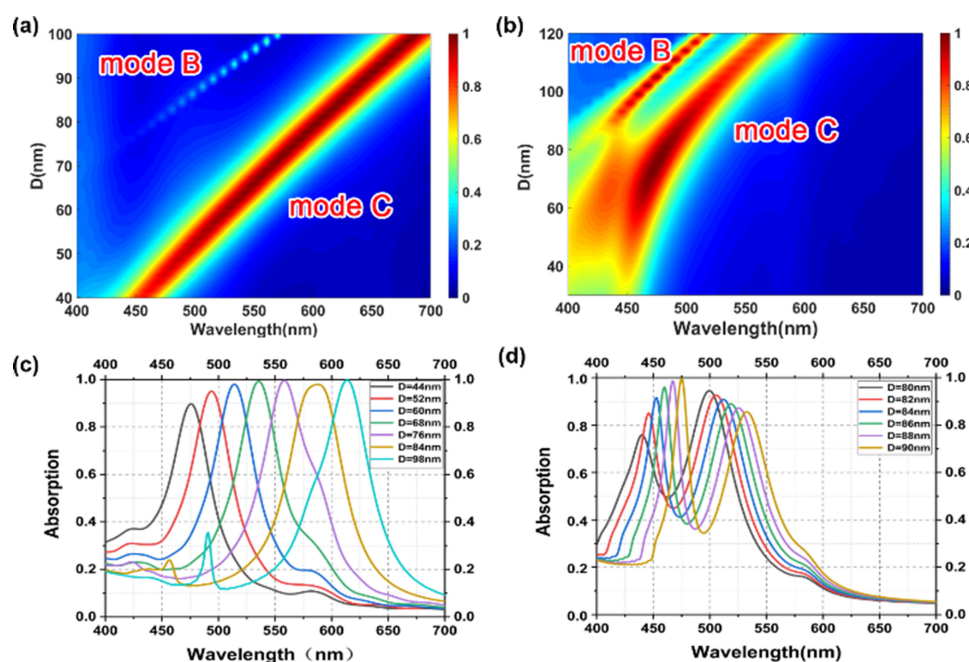
Haigui Yang

Xiaoyi Wang

Tongtong Wang

Yanchao Wang

Jinsong Gao



DOI: 10.1109/JPHOT.2021.3060460

Tunable Perfect Absorption Structures Based on Cavity Coupling and Plasmon Hybrid Mode

Yuanhang Zhao^{1,2}, Zizheng Li,¹ Qiang Li,¹ Kun Wang,^{1,2}
Jinbo Gao,^{1,2} Ke Wang,^{1,2} Haigui Yang,¹ Xiaoyi Wang,¹
Tongtong Wang,¹ Yanchao Wang,¹ and Jinsong Gao^{1,2,3}

¹Key Laboratory of Optical System Advanced Manufacturing Technology, Changchun Institute of Optics, Fine Mechanics and Physics, Chinese Academy of Sciences, Changchun 130033, China

²University of the Chinese Academy of Sciences, Beijing 100039, China

³Jilin Provincial Key Laboratory of Advanced Optoelectronic Equipment and Instrument Manufacturing Technology, Changchun 130033, China

DOI:10.1109/JPHOT.2021.3060460

This work is licensed under a Creative Commons Attribution 4.0 License. For more information, see <https://creativecommons.org/licenses/by/4.0/>

Manuscript received August 19, 2020; revised January 23, 2021; accepted February 16, 2021. Date of publication February 19, 2021; date of current version March 12, 2021. This work was supported by the National Natural Science Foundation of China under Grants 61705226, 61905238, 61875193, and 61675199. Corresponding authors: Zizheng Li; Qiang Li (e-mail: lizizheng@ciomp.ac.cn; liqiang@ciomp.ac.cn).

Abstract: We report a theoretical study of a perfect absorber based on the metal-insulator-metal (MIM) structure, which achieves perfect absorption of single and double peaks in the visible range. The top Ag and middle SiO₂ are arranged in a periodic nanopillar array. Adjusting the structural parameters of the nanopillars to indirectly control the absorption spectrum, theoretically the maximum single-peak absorption can reach more than 99.0% and the maximum double-peak absorption can reach more than 90.0%. We investigate its absorption mechanism through simulations and calculations, and explain the results well with the SPP scattering mode and F-P cavity theory. We find that through the double-peak absorption process, the mode split phenomenon appears as the thickness of SiO₂ increases. Therefore, the selective appearance of absorption peaks can be achieved, which provides the possibility of application in absorbers.

Index Terms: MIM structure, Surface plasmon polariton, F-P cavity, perfect absorber.

1. Introduction

Plasmonics is one of the research hotspots in nanophotonics. Its main concern is to realize the transfer of electromagnetic radiation energy at the interface between metal and dielectric using microstructures. Studying the interaction between light and matter with the help of microscopic fields opens up a new perspective for us [1]–[4]. Surface plasmon polariton (SPP) is an electromagnetic wave that propagates along the interface between metal and dielectric. It has been shown to exhibit the characteristics of strong enhancement of local field and large in-plane momentum [5]. It can effectively confine the energy of a photon in a very thin area, which shows a trend of attenuation along the vertical direction of the interface [6]–[9]. Furthermore, the wave vector of SPPs is relatively long, which can break the diffraction limit [10]. The SPP around the nanostructure

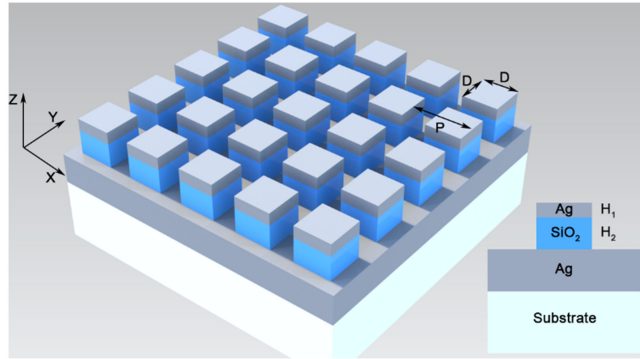


Fig. 1. Conceptual illustration of the three-layered MIM absorber structure.

has unique and significant manipulability to light. This makes it useful in biochemical sensors [11], energy harvesting [12]–[15], nonlinear optics [16]–[18], and solar batteries [19], [20].

Perfect absorption [12] has attracted much attention for its important applications in the fields of thermal radiation [20], photodetectors [21], [22], nonlinear [23], and sensing [24]–[26]. Many theoretical and experimental works concerning perfect absorption based on plasmonic mode have been demonstrated in recent years. To achieve selective perfect absorption, various nanostructures such as metal grating [27]–[32], nanopore array [33]–[35], nanopillar array [36]–[38], and nanosphere [39] have been investigated, whose shape, size, materials, and dielectric environment can significantly affect the spectral bands [40]. When an electromagnetic wave propagates through a nanostructured surface, it may change its phase, amplitude, polarization, or coherence. This can lead to many exotic electromagnetic phenomena, and allows the electromagnetic response to be almost completely controlled by the researchers [41]. Among these plasmonic structures, the metal-insulator-metal (MIM) structure is one of the most common structural units [42]. It exhibits excellent characteristics, such as spectral tunability and almost perfect absorption [43], [44]. The spectrum of the MIM can be easily tuned by changing the metal and dielectric layer thicknesses [45]. Combining MIM and plasmonic in the same platform has provided new paradigms for perfect absorption. The resulting nanostructured MIM absorber has converted metal losses into advantages [46]–[49].

In this article, a triple MIM layer structure is mainly proposed and studied. By designing the structure parameters, tunable perfect absorption can be achieved at the resonant wavelength in the visible region. Fig. 1 is the schematic diagram of the proposed MIM structure. A periodical nanopillar array of SiO_2 and silver (Ag) is arranged on the bottom Ag layer with a thickness of 100 nm, in which the thickness of top Ag layer and SiO_2 are H_1 and H_2 , respectively. The width and period of the nanopillar array are D and P . Silver was chosen because of its high reflectivity in the visible range. This ensures a high absorption only at the resonance wavelengths; the SiO_2 dielectric layer was selected because of its high transmission and stability in the visible region. By designing the structure parameters of the nanostructure, the highest absorption in the visible range can be achieved. Moreover, we further explored the double-peak absorption and its physical mechanism. Because of its excellent ability to control the light field, which has great potential value in the field of optical sensing and nonlinear optics

2. Results and Discussions

The finite-difference time-domain (FDTD) simulation tool was used to simulate the absorption characteristics of the absorber under plane wave with normal incidence. We set the periodic boundary condition in the X and Y directions. In the z -direction, we use the perfectly matched layer (PML) condition for obtaining absorption (A). We use a high mesh accuracy to ensure the convergence of the simulation. The duty cycle of the nanopillar array is defined as the ratio of the

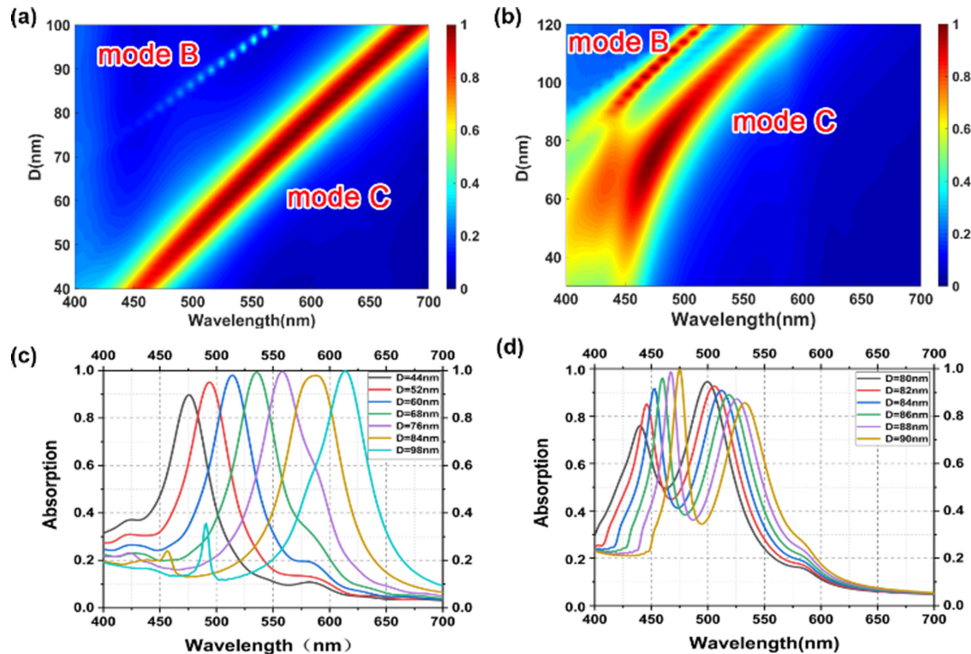


Fig. 2. (a) $H_1 = 20\text{ nm}$ and (b) $H_1 = 70\text{ nm}$, the simulated two-dimensional profile of absorption spectrum, duty ratio = 0.2, SiO_2 thickness $H_2 = 48\text{ nm}$; (c) side length of nanopillar structure $D = 44\text{ nm}, 52\text{ nm}, 60\text{ nm}, 68\text{ nm}, 76\text{ nm}, 84\text{ nm}, \text{ and } 92\text{ nm}$; (d) side length of the nanopillar structure $D = 80\text{ nm}, 82\text{ nm}, 84\text{ nm}, 86\text{ nm}, 88\text{ nm}$ and 90 nm absorption spectrum.

side length to the period (D/T). With the fixed duty ratio 1/5 and the intermediate dielectric SiO_2 thickness $H_2 = 48\text{ nm}$, we sweep the side length D from 40 nm to 100 nm with an interval of 2 nm using the FDTD simulation. Finally, the simulated absorption is shown in Figs. 2(a) and 2(b). Since the bottom silver layer is much thicker than its skin depth, transmitted light will be completely suppressed ($T = 0$). According to $A + T + R = 1$, when the transmittance is 0, $A + R = 1$, so the absorption characteristics of the structure can be determined by the reflection spectrum, as shown in Figs. 2(c) and 2(d). In Fig. 2(a), a strong mode C appears in the visible range. When the side length D increases to around 78 nm, a very weak mode B appears leading to a strong absorption peak. As the side length D increases, both the strong and weak absorption peaks produce a significant red shift. Fig. 2(c) shows the absorption spectra when the side length D are 44 nm, 52 nm, 60 nm, 68 nm, 76 nm, 84 nm, and 92 nm, respectively. When the duty cycle D/T is fixed, the maximum value of the absorption peak corresponding to the resonance wavelength moves from 475 nm to 613 nm. After the side length D is increased to 60 nm, the maximum absorption will reach more than 99%, which achieves perfect absorption. As we can see from Figs. 2(a) and 2(b), when the thickness of the upper layer silver H_1 increases from 20 nm to 70 nm, the intensity of mode B is significantly improved. When the side length D is greater than 78 nm, two absorption peaks can be obtained in the visible range, as shown in Fig. 2(d). Based on this mechanism, it is expected to achieve single-peak and double-peak selective absorption in the visible range.

The effect of the intermediate dielectric SiO_2 thickness on the absorption are further explored using FDTD simulation. Firstly, the side length D and period P are fixed as 84 nm and 420 nm, respectively. The absorption of the proposed structure array is shown in Figs. 3(a) and 3(b), which indicates that the thickness of the upper silver H_1 are 20 nm and 70 nm, respectively. It is found that the effect of mode B gets stronger when the thickness H_1 increases. In addition, the resonance wavelength of mode B does not change with the thickness of the upper Ag and the intermediate layer SiO_2 . For mode C , blue shift occurs when the thickness of upper Ag layer and intermediate layer increases.

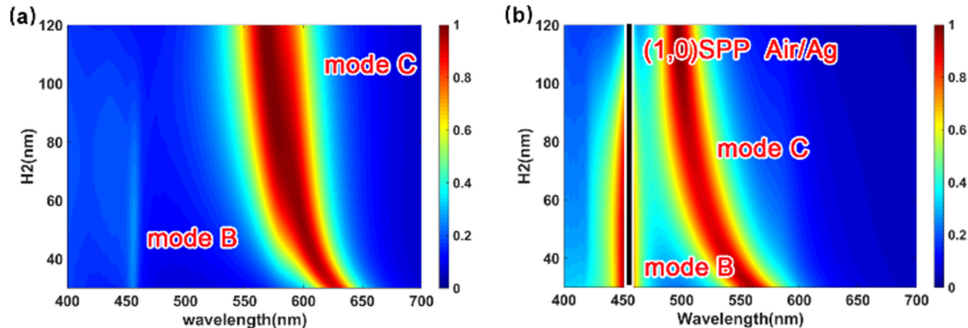


Fig. 3. The side length D of the nanopillar is 84 nm, the period P is 420 nm, and the thickness H_1 of the upper Ag is (a) 20 nm and (b) 70 nm.

To reveal the physical mechanism of spectral selective, we take the structure parameters in Fig. 3(b) as an example. It can be seen that mode B is affected by the period, size, and structure thickness. In according to previous works, the resonance wavelength of the SPPs is affected by the period and the angle of incidence. The dispersion formula for the SPPs transmitted along the interface of two half-spaces can be expressed as [50]:

$$\lambda_{spp} = \frac{P}{\sqrt{i^2 + j^2}} \sqrt{\frac{\varepsilon_m \varepsilon_d}{\varepsilon_m + \varepsilon_d}} \quad (1)$$

where λ_{spp} corresponds to resonance wavelength in SPPs, P is the period of the structure, and i, j are resonance orders. We know that only if $\lambda = \lambda_{spp}$, the energy carried by the incident electromagnetic wave can be transferred to the interface between the metal and the dielectric. By the calculation, mode B can be assigned to the (1, 0) SPP mode propagating at the air-Ag interface as shown by the black line in Fig. 3(b).

Mode C has an obvious blue shift phenomenon as the thickness of H_2 increases. For the MIM structure, as we know, the thickness of the SiO_2 layer H_2 can effectively affect the mode in the cavity. F-P cavity resonance can form between the upper silver and the lower silver. The waveguide resonance condition corresponding to the F-P cavity can be expressed as [51]–[53]:

$$2\beta D + \varphi = 2m\pi \quad (2)$$

where β is the complex propagation constant, D is the side length of the nanopillar structure, m is the resonance order, and φ is the phase shift of the propagating wave on both sides of the waveguide. By means of the formula of the resonance condition, we use β to obtain the resonance order m . We can obtain β via the following dispersion equation [54]:

$$\begin{aligned} \varepsilon_d k_m + \varepsilon_m k_d \tanh \left(\frac{k_d H_2}{2} \right) &= 0 \\ \beta^2 - \varepsilon_d k_0^2 &= k_d^2 \\ \beta^2 - \varepsilon_m k_0^2 &= k_m^2 \end{aligned} \quad (3)$$

where ε_d is the dielectric constant of SiO_2 , ε_m is the dielectric constant of Ag, H_2 is the thickness of SiO_2 , and $k_0 = 2\pi/\lambda_0$ is the free space wave vector. Combining the above formulas, we can obtain the β value and the resonance order m ($m = 1$). Different propagation wavelengths will produce different phase shifts. The phase shifts φ for different SiO_2 thicknesses at the resonance wavelengths can be calculated, and the function between SiO_2 thickness and phase shift can be obtained by fitting as shown in Fig. 4(a). The effective refractive index of a MIM waveguide is

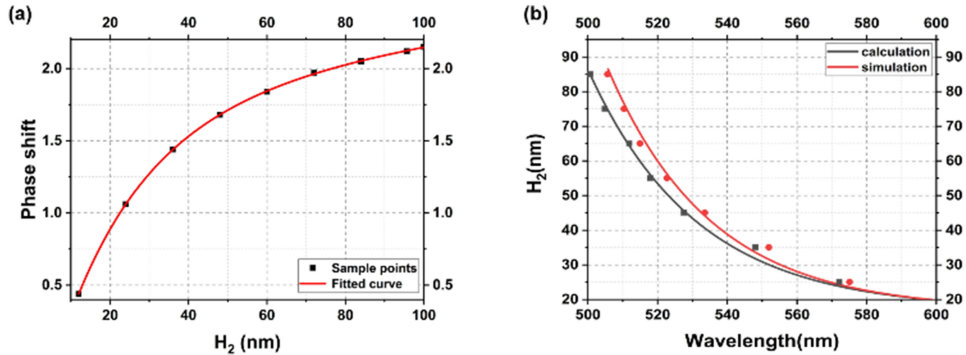


Fig. 4. (a) Linear fitting function between SiO_2 thickness and phase shift; (b) comparison of calculation results and simulation results.

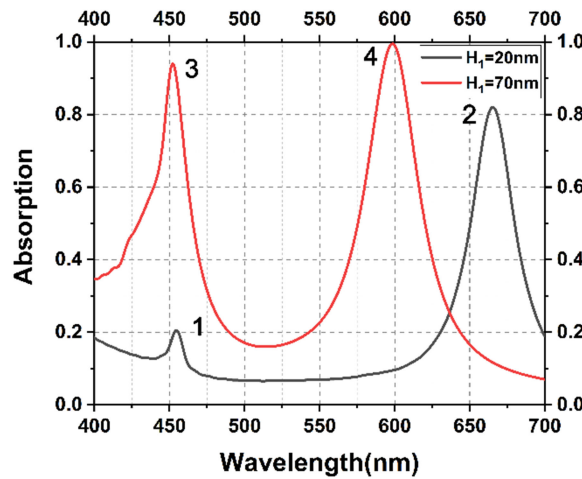


Fig. 5. Comparison of absorption spectrum when $H_2 = 20\text{ nm}$ and $H_1 = 70\text{ nm}$ and 20 nm , respectively.

defined as $n_e = \beta/k_0$, so the expression of the resonance wavelength can be expressed as [55]:

$$\lambda_r = \frac{2Dn_e}{[m - (\varphi/2\pi)]} \quad (4)$$

where $D = 84\text{ nm}$ and $m = 1$. When determining the equivalent refractive index n_e and phase shift φ , we can get the resonance wavelength. The phase shift φ can be obtained from the fitted curve, and the equivalent refractive index is obtained by (3). The comparison between calculation results and simulation results is shown in Fig. 4(b), which shows the results obtained by FDTD simulation and dispersion model are in good agreement. The calculation results can confirm that the resonance wavelength shifts to shorter wavelength with the increase of the SiO_2 layer thickness H_2 .

Fig. 2(a) shows that mode B appears in the visible range when the parameter of nanostructure reaches a certain size. We have compared the absorption curves when the thickness of upper Ag layer H_1 are 20 nm and 70 nm as shown in Fig. 5. There are two absorption peaks in the visible range, which are caused by mode B and mode C , respectively. Compared to absorption peak 2, the effect of absorption peak 1 is almost negligible. It is interested that when the thickness of Ag layer H_1 is 70 nm , there are two absorption peaks indicated 3 and 4 whose maximum absorption can reach more than 90%. Therefore, we can achieve double-peak absorption in the visible range by adjusting the structure parameters of the nanopillar.

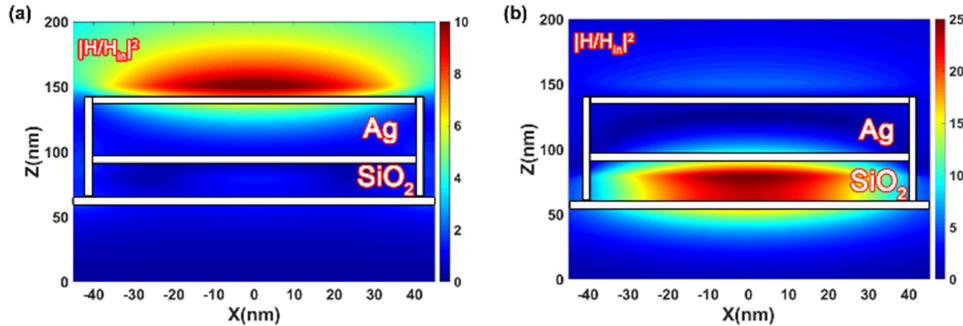


Fig. 6. Distribution of magnetic field intensity at resonance wavelength (a) $\lambda_3 = 451 \text{ nm}$ and (b) $\lambda_4 = 600 \text{ nm}$.

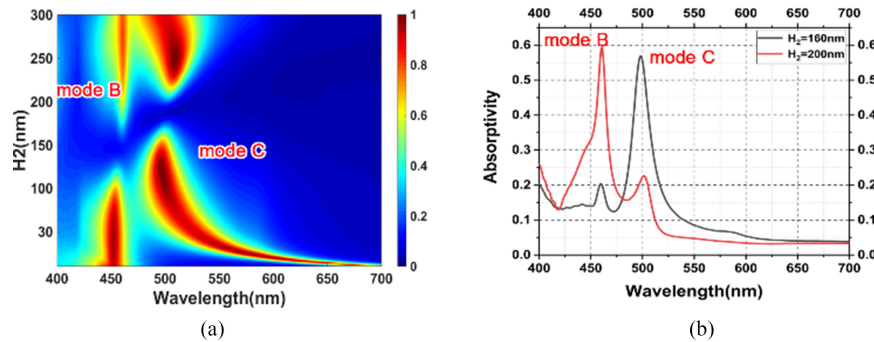


Fig. 7. Scanning chart of the thickness of the upper silver layer H_1 at (a) 70 nm, the thickness of the intermediate dielectric layer H_2 from 10 to 300 nm; (b) when the thickness of SiO_2 H_2 is adjusted to 160 nm and 200 nm, the modes B and C appear separated.

In order to further clarify the physical mechanism of the wavelength selective characteristic, we studied the magnetic field distributions at the resonant wavelength ($\lambda_3 = 451 \text{ nm}$, $\lambda_4 = 600 \text{ nm}$) when the thickness of upper Ag layer H_1 is 70 nm as shown in Fig. 6. The distribution of magnetic field intensity shown in Fig. 6(a) is located at the interface of the air and upper Ag layer, which indicates that the incident wave excites the SPP mode at the Air/Ag interface. While in Fig. 6(b), the distribution of the magnetic field is located in the cavity of SiO_2 layer, which indicates that the mode C is a typical F-P cavity resonance. The analysis of the physical generation mechanism of each absorption peak is helpful to explore the proposed structure further, and also provides a strong support for the reliability of the theoretical analysis in the study.

In Fig. 3(b), it is found that when the thickness of SiO_2 dielectric layer H_2 increases, mode B tends to disappear. To confirm it further, we increased the simulated range of SiO_2 thickness from 10 nm to 300 nm. When the SiO_2 thickness H_2 is in the range of 125 nm to 160 nm, mode B disappears, while when the thickness H_2 is in the range of 180 nm to 205 nm, mode C disappears, which lead to the split of the original continuous mode as shown in Fig. 7(a). It means that the selective appearance of two absorption peaks can be obtained by controlling the thickness of SiO_2 layer H_2 as shown in Fig. 7(b). In the meanwhile, if the thickness H_2 is equal to 160 nm, mode B is in the “off” state, and mode C is in the “on” state, while if the thickness H_2 is equal to 200 nm, mode C is in the “off” state, and mode B is in the “on” state, which make it possible to be applied as perfect absorbers in the visible range.

Using FDTD to simulate the electric field distribution near the fractures of modes B and C, the electric field distribution along the z-direction can be obtained. The thickness of the intermediate dielectric layer H_2 for mode B fracture are 112 nm and 188 nm, while the thickness H_2 for mode C fracture are 162 nm and 212 nm, as shown in Fig. 8. It can be clearly seen that the electric

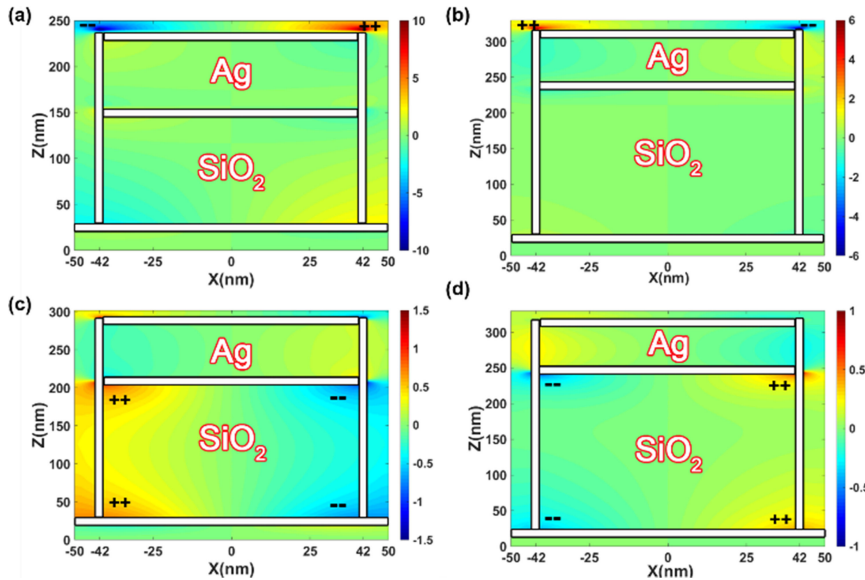


Fig. 8. The electric field distribution along the z -direction when the thickness of the intermediate dielectric layer H_2 is (a) 112 nm, (b) 188 nm, (c) 162 nm, and (d) 212 nm, respectively, corresponding to the resonance wavelengths near the two mode fractures.

field phase has changed by π near the fracture of the mode split. This shows that as the thickness of the intermediate dielectric layer H_2 increases, the electric fields of mode B and mode C both change direction, which also means the moment from negative to positive will inevitably appear as '0'. Therefore, in the process of increasing the thickness of the intermediate H_2 dielectric layer, there must be a mode split, such as in Fig. 7.

3. Conclusion

In summary, we show a mechanism of single and double peak absorption in the visible range based on the MIM structure. The resonance wavelength was calculated by the SPP mode dispersion, F-P cavity resonance conditions. The calculated results were in good agreement with the FDTD simulation results, which verified the validity of our theory and simulation. The energy captured by these resonance modes will be dissipated through dielectric loss or ohmic loss, that is, the incident light absorbed by the absorbed body will eventually be converted into dissipated heat, thus achieving super absorption at a specific wavelength. Theoretically, the single-peak absorption can reach more than 99.0% achieving perfect absorption, and the double-peak absorption can reach 90.0%. We analysed the SPP mode and F-P cavity mode supported by the MIM structure in details, and explained the relationship between each absorption peak and the two modes. Based on the phenomenon that the mode disappears as the SiO_2 thickness H_2 increases, the selective appearance of absorption peaks can be controlled, which provides the possibility of application in the visible range. And provides theoretical support for applications in optical sensing and other fields.

References

- [1] A. Dhibi, M. Khemiri, and M. Oumezzine, "Theoretical study of surface plasmons coupling in transition metallic alloy 2D binary grating," *Physica E-Low-Dimensional Syst. Nanostructures*, vol. 79, pp. 160–166, 2016.
- [2] R. Hillenbrand, T. Taubner, and F. Keilmann, "Phonon-enhanced light-matter interaction at the nanometre scale," *Nature*, vol. 418, no. 6894, pp. 159–162, 2002.

- [3] C. Koechlin, P. Bouchon, F. Pardo, J. L. Pelouard, and R. Haidar, "Analytical description of subwavelength plasmonic MIM resonators and of their combination," *Opt. Exp.*, vol. 21, no. 6, pp. 7025–7032, 2013.
- [4] T. Allsop *et al.*, "Photonic gassensors exploiting directly the optical properties of hybrid carbon nanotube localized surface plasmon structures," *Light Sci. Appl.*, vol. 5, no. 2, 2016, Paper. e16036.
- [5] L. Huang *et al.*, "Helicity dependent directional surface plasmon polariton excitation using a metasurface with interfacial phase discontinuity," *Light Sci. Appl.*, vol. 2, no. 3, 2013, Paper. e70.
- [6] C. F. Guo, T. Sun, F. Cao, Q. Liu, and Z. Ren, "Metallic nanostructures for light trapping in energy-harvesting devices," *Light Sci. Appl.*, vol. 3, no. 4, 2014, Paper. e161.
- [7] Q. Min and R. Gordon, "Surface plasmon microcavity for resonant transmission through a slit in a gold film," *Opt. Exp.*, vol. 16, no. 13, pp. 9708–9713, 2008.
- [8] K. Wu, T. Rindzevicius, M. S. Schmidt, K. B. Mogensen, S. Xiao, and A. Boisen, "Plasmon resonances of Ag capped Si nanopillars fabricated using mask-less lithography," *Opt. Exp.*, vol. 23, no. 10, pp. 12965–12978, 2015.
- [9] Y. Zhu, X. Hu, H. Yang, and Q. Gong, "On-chip plasmon-induced transparency based on plasmonic coupled nanocavities," *Sci. Rep.*, vol. 4, no. 1, pp. 3752–3752, 2015.
- [10] D. K. Gramotnev and S. I. Bozhevolnyi, "Nanofocusing of electromagnetic radiation," *Nat. Photon.*, vol. 8, no. 1, pp. 13–22, 2014.
- [11] A. Cattoni *et al.*, " $\lambda^3/1000$ plasmonic nanocavities for biosensing fabricated by soft UV nanoimprint lithography," *Nano Lett.*, vol. 11, no. 9, pp. 3557–3563, 2011.
- [12] C. M. Watts, X. L. Liu, and W. J. Padilla, "Metamaterial electromagnetic wave absorbers," *Adv. Mater.*, vol. 24, no. 23, pp. 98–120, 2012.
- [13] Y. Qu *et al.*, "Spatially and spectrally resolved narrowband optical absorber based on 2D grating nanostructures on metallic films," *Adv. Opt. Mater.*, vol. 4, no. 3, pp. 480–486, 2016.
- [14] T. Cao, C. Wei, R. E. Simpson, L. Zhang, and M. J. Cryan, "Broadband polarization-independent perfect absorber using a phase-change metamaterial at visible frequencies," *Sci. Rep.*, vol. 4, no. 1, pp. 3955–3955, 2015.
- [15] K. Liu *et al.*, "A large-scale lithography-free metasurface with spectrally tunable super absorption," *Nanoscale*, vol. 6, no. 11, pp. 5599–5605, 2014.
- [16] A. Popov, "Nonlinear optics of backward waves and extraordinary features of plasmonic nonlinear-optical microdevices," *Eur. Phys. J. D*, vol. 58, no. 2, pp. 263–274, 2010.
- [17] M. W. Klein, M. Wegener, N. Feth, and S. Linden, "Experiments on second- and third-harmonic generation from magnetic metamaterials," *Opt. Exp.*, vol. 15, no. 8, pp. 5238–5247, 2008.
- [18] R. A. Pala, J. White, E. Barnard, J. Liu, and M. L. Brongersma, "Design of plasmonic thin-film solar cells with broadband absorption enhancements," *Adv. Mater.*, vol. 21, no. 34, pp. 3504–3509, 2009.
- [19] V. E. Ferry, L. A. Sweatlock, D. Pacifici, and H. A. Atwater, "Plasmonic nanostructure design for efficient light coupling into solar cells," *Nano Lett.*, vol. 8, no. 12, pp. 4391–4397, 2008.
- [20] Y. Xuan, "An overview of micro/nanoscaled thermal radiation and its applications," *Photon. Nanostructures: Fundamentals Appl.*, vol. 12, no. 2, pp. 93–113, 2014.
- [21] H. Chalabi, D. Schoen, and M. L. Brongersma, "Hot-electron photodetection with a plasmonicnanostripe antenna," *Nano Lett.*, vol. 14, no. 3, pp. 1374–1380, 2014.
- [22] M. Abutoama *et al.*, "Ultrahigh field enhancement optimization versus rabi splitting investigated using au nanobipyramids on metal film," *J. Phys. Chem. C*, vol. 123, no. 20, pp. 12984–12996, 2019.
- [23] N. *et al.*, "Ultra-broadband enhancement of nonlinear optical processes from randomly patterned super absorbing metasurfaces," *Sci. Rep.*, vol. 7, no. 1, 2017, Art. no. 4346.
- [24] B. Park *et al.*, "Surface plasmon excitation in semitransparent inverted polymer photovoltaic devices and their applications as label-free optical sensors," *Light Sci. Appl.*, vol. 3, no. 12, 2014, Paper. e222.
- [25] X. Liu, J. Gao, J. Gao, H. Yang, X. Wang, T. Wang, Z. Shen, Z. Liu, H. Liu, J. Zhang, Z. Li, Y. Wang, and Q. Li, "Microcavity electrodynamics of hybrid surface plasmon polariton modes in high-quality multilayer trench gratings," *Light Sci. Appl.*, vol. 7, no. 14, pp. 1–10, 2018.
- [26] J. Gao, N. Zhang, D. Ji, H. Song, and Q. Gan, "Superabsorbing metasurfaces with hybrid Ag-Au nanostructures for surface-enhanced raman spectroscopy sensing of drugs and chemicals," *Small Methods*, vol. 5, 2018, Art. no. 1800045.
- [27] N. Zhang *et al.*, "Ultrabroadband metasurface for efficient light trapping and localization: A universal surface-enhanced raman spectroscopy substrate for 'All' excitation wavelengths," *Adv. Mater. Interfaces*, vol. 2, 2015, Art. no. 1500142.
- [28] L. Meng, D. Zhao, Z. Ruan, Q. Li, Y. Yang, and M. Qiu, "Optimized grating as an ultra-narrow band absorber or plasmonic sensor," *Opt. Lett.*, vol. 39, no. 5, pp. 1137–1140, 2014.
- [29] S. Luo, J. Zhao, D. Zuo, and X. Wang, "Perfect narrow band absorber for sensing applications," *Opt. Exp.*, vol. 24, no. 9, pp. 9288–9294, 2016.
- [30] D. Wu *et al.*, "Infrared perfect Ultra-narrow band absorber as plasmonic sensor," *Nanoscale Res. Lett.*, vol. 11, no. 1, pp. 483–483, 2016.
- [31] Y.-T. Yoon *et al.*, "Color filter incorporating a subwavelength patterned grating in poly silicon," *Opt. Exp.*, vol. 16, no. 4, pp. 2374–2380, 2008.
- [32] F. Cheng, X. Yang, D. Rosenmann, L. Stan, D. Czaplewski, and J. Gao, "Enhanced structural color generation in aluminum metamaterials coated with a thin polymer layer," *Opt. Exp.*, vol. 23, no. 19, pp. 25329–25339, 2015.
- [33] F. Cheng, J. Gao, L. Stan, D. Rosenmann, D. Czaplewski, and X. Yang, "Aluminum plasmonic metamaterials for structural color printing," *Opt. Exp.*, vol. 23, no. 11, pp. 14552–14560, 2015.
- [34] Z. Fang, Y.-R. Zhen, L. Fan, X. Zhu, and P. Nordlander, "Tunable wide-angle plasmonic perfect absorber at visible frequencies," *Phys. Rev. B*, vol. 85, no. 24, 2012, Art. no. 245401.
- [35] Y. Li, B. An, S. Jiang, J. Gao, Y. Chen, and S. Pan, "Plasmonic induced triple-band absorber for sensor application," *Opt. Exp.*, vol. 23, no. 13, pp. 17607–17612, 2015.
- [36] H. Qian, S. Li, C.-F. Chen, S.-W. Hsu, S.E. Bopp, Q. Ma, A.R. Tao, and Z. Liu, "Large optical nonlinearity enabled by coupled metallic quantum wells," *Light Sci. Appl.*, vol. 8, no. 13, pp. 1–7, 2019.

- [37] J. Hao, J. Wang, X. Liu, W. J. Padilla, L. Zhou, and M. Qiu, "High performance optical absorber based on a plasmonic metamaterial," *Appl. Phys. Lett.*, vol. 96, no. 25, 2010, Art. no. 251104.
- [38] S. L. Diederhofen, O. T. Janssen, G. Grzela, E. P. Bakkers, and J. G. Rivas, "Strong geometrical dependence of the absorption of light in arrays of semiconductor nanowires," *ACS Nano*, vol. 5, no. 3, pp. 2316–2323, 2011.
- [39] F. Pincella, K. Isozaki, and K. Miki, "A visible light-driven plasmonic photocatalyst," *Light Sci. Appl.*, vol. 3, no. 1, 2014, Paper. e133.
- [40] X.-C. Ma, Y. Dai, L. Yu, and B.-B. Huang, "Energy transfer in plasmonic photocatalytic composites," *Light Sci. Appl.*, vol. 5, no. 2, 2016, Paper. e16017.
- [41] C. M. Watts, X. Liu, and W. J. Padilla, "Metamaterial electromagnetic wave absorbers," *Adv. Mater.*, vol. 24, no. 23, pp. 98–120, 2012.
- [42] B. C. Pan, H. C. Zhang, and T. J. Cui, "Multilayer transmissions of spoof surface plasmon polaritons for multifunctional applications," *Adv. Mater. Technol.*, vol. 2, no. 1, 2017, Art. no. 1600159.
- [43] P. Bouchon, C. Koechlin, F. Pardo, R. Haidar, and J.-L. Pelouard, "Wideband omnidirectional infrared absorber with a patchwork of plasmonic nanoantennas," *Opt. Lett.*, vol. 37, no. 6, pp. 1038–1040, 2012.
- [44] J. Yang, C. Sauvan, A. Jouanin, S. Collin, J. L. Pelouard, and P. Lalanne, "Quality factor of 3D metal-insulator-metal nanoresonators," in *Proc. 7th Int. Congr. Adv. Electromagn. Mater. Microw. Opt.*, 2013, pp. 397–399.
- [45] K. Q. Le, Q. M. Ngo, and T. K. Nguyen, "Nanostructured metal-insulator-metal metamaterials for refractive index biosensing applications: Design, fabrication, and characterization," *IEEE J. Sel. Topics Quantum Electron.*, vol. 23, no. 2, pp. 388–393, Mar./Apr. 2017.
- [46] C. Argyropoulos, K. Q. Le, N. Mattiucci, G. D'Aguanno, and A. Alu, "Broadband absorbers and selective emitters based on plasmonic brewster metasurfaces," *Phys. Rev. B*, vol. 87, no. 20, 2013, Art. no. 205112.
- [47] K. Q. Le and J. Bai, "Enhanced absorption efficiency of ultrathin metamaterial solar absorbers by plasmonic Fano resonance," *J. Opt. Soc. Amer. B*, vol. 32, no. 4, pp. 595–600, 2015.
- [48] M. Farhat, T.-C. Cheng, K. Q. Le, M. M. Cheng, H. Bagci, and P. Chen, "Mirror-backed dark alumina: A nearly perfect absorber for thermoelectronics and thermophotovoltaics," *Sci. Rep.*, vol. 6, no. 1, 2016, Art. no. 19984.
- [49] M. Farhat, M. M. Cheng, K. Q. Le, and P.-Y. Chen, "Nanoantenna harmonic sensor: Theoretical analysis of contactless detection of molecules with light," *Nanotechnology*, vol. 26, no. 41, 2015, Art. no. 415201.
- [50] W. L. Barnes, A. Dereux, and T. W. Ebbesen, "Surface plasmon subwavelength optics," *Nature*, vol. 424, no. 6950, pp. 824–830, 2003.
- [51] G. David *et al.*, "Coupling of surface plasmon polariton in Al-doped ZnO with Fabry-Perot resonance for total light absorption," *Photonics*, vol. 4, no. 4, pp. 35–35, 2017.
- [52] J. Jiang, Y. B. Xie, Z. Y. Liu, X. M. Tang, X. J. Zhang, and Y. Y. Zhu, "Amplified spontaneous emission via the coupling between Fabry-Perot cavity and surface plasmon polariton modes," *Opt. Lett.*, vol. 39, no. 8, pp. 2378–2381, 2014.
- [53] V. I. Belotelov, A. N. Kalish, A. K. Zvezdin, A. V. Gopal, and A. S. Vengurlekar, "Fabry-Perot plasmonic structures for nanophotonics," *J. Opt. Soc. Amer. B*, vol. 29, no. 3, pp. 294–299, 2012.
- [54] F. Hu, H. Yi, and Z. Zhou, "Band-pass plasmonic slot filter with band selection and spectrally splitting capabilities," *Opt. Exp.*, vol. 19, no. 6, pp. 4848–4855, 2011.
- [55] X. Liu, J. Gao, H. Yang, X. Wang, S. Tian, and C. Guo, "Hybrid plasmonic modes in multilayer trench grating structures," *Adv. Opt. Mater.*, vol. 5, no. 22, 2017, Art. no. 1700496.